IEEE Access
Multidisciplinary | Rapid Review | Open Access Journal

Received January 27, 2022, accepted March 11, 2022, date of publication March 17, 2022, date of current version March 24, 2022.

Digital Object Identifier 10.1109/ACCESS.2022.3160459

A Method to Co-Design Antenna Element and Array Patterns

RIKU KORMILAINEN[1], ANU LEHTOVUORI[1], JUUSO LIESIÖ[2], AND VILLE VIIKARI[1], (Senior Member, IEEE)

[1]Department of Electronics and Nanoengineering, Aalto University School of Electrical Engineering, 02150 Espoo, Finland
[2]Department of Information and Service Management, Aalto University School of Business, 02150 Espoo, Finland

Corresponding author: Riku Kormilainen (riku.kormilainen@aalto.fi)

The work of Riku Kormilainen was supported by the Aalto University School of Electrical Engineering (ELEC) Doctoral School.

ABSTRACT In this paper, we develop a novel method to design the elements of an antenna array and their feed weights simultaneously. The method is based on formulating the design problem as a non-linear multi-objective optimization model that estimates the realized gain at certain angles as a function of the element-level port signals and impedances, and the array-level weights for the elements. This enables utilization of genetic algorithms to find optimal signals, impedances, and weights for given steering range requirements. As an example, an array consisting of multi-port antenna elements is simulated and modeled with its impedance and radiation matrices. These matrices are used in the calculation of realized gain with the model. The model is then applied as part of the method to find as wide scanning range for the array as possible. The antenna elements are designed such that the multi-port system can be reduced to a single feed with physically realizable matching components and a matching network. The array designed with the proposed method is also compared to a reference antenna array of the same size. Both the simulations and measurements verify that the method can provide substantial improvements in the scanning range as compared to the reference.

INDEX TERMS Antenna arrays, antenna radiation patterns, Pareto optimization methods, phased arrays.

I. INTRODUCTION

Antenna arrays have an increasing role in modern mobile communication. Currently, 5G networks are being deployed all around the world. Especially, the phased array antennas are an ideal option for implementing the wireless communication for those networks [1] because of their versatile beamforming capabilities. The beamforming capabilities of these antennas should be designed to different goals, such as achieving a pre-defined gain at certain angular range with low side lobe levels. Thus, there is a need for systematic design methods for those arrays.

One of the trends in the current antenna array research is element-driven design [2]–[7] which aims to find a suitable element for the antenna array. Common design goals for these elements include wide impedance matching [2], [3], a wide beam pattern [2]–[4], or a reconfigurable beam pattern [5] to achieve wide matching and/or wide angle beam steering for the array. Typical for these design approaches is their iterative nature which requires numerous and laborious electromagnetic (EM) simulations. A single element is designed with one set of EM-simulations after which another possible set of EM-simulations is required to adjust the individual elements to perform well as part of an array. One possible solution for reducing required EM-simulations is to design the single element as part of an infinite array [6], [7]. However, this approach is mainly suitable for large arrays since the edge effects of a finite array cannot be directly taken into account. Furthermore, this approach also assumes a conventional array feeding scheme where all the elements are fed with uniform amplitudes and progressive phase shifts.

Another research trend concentrates on the array-driven design [8]–[16] in which the goal is to optimize array-level properties such as directivity, array pattern shape, and side-lobe levels (SLL). There are numerous methods for optimizing these properties. For example, methods to design sub-arrays have been proposed [8], [9]. These methods first divide array elements into groups, and then, they aim to find

The associate editor coordinating the review of this manuscript and approving it for publication was Debdeep Sarkar.

optimal groups, and array weights. There are also methods to design the power pattern of an array by properly choosing the array weights [10]–[12]. Furthermore methods for designing sparse arrays exist, see e.g. [13], [14]. Generally, the goal of sparse array designs is minimizing the number of elements in an antenna array while maintaining some pre-defined constraints such as reasonably low SLL. The trade-off of these methods is that they rarely consider the antenna element properties, such as physical dimensions, as design variables although there are techniques to consider the mutual coupling between elements and active element patterns in the array optimization.

Several studies [10], [14], [15] incorporate the active element patterns and mutual coupling as part of the optimization process through EM-simulations. These approaches do not take element-level variables into account but could possibly be extended to do so. In [16], a semi-analytical method is proposed to design the element factors of multi-port overlapped sub-arrays based on a single active and multiple reactively loaded passive waveguide elements. However, this method assumes separable array and element patterns.

The aforementioned sub-array methods can be seen as methods that utilize multi-port antenna elements as part of the array. However, the current literature does not offer generalized methods that can optimize the realized gain for this kind of array from either simulated or measured scattering parameters and port-specific electric far fields.

Motivated by this gap in the existing literature, we propose a novel method that enables the simultaneous design of both the individual elements and the entire array. The method is based on deriving a new non-linear multi-objective optimization model for realized gain that is dependent on element-level port signals and impedances, and array-level weights.

To illustrate the use of the developed multi-objective optimization model, we apply the method for a 3 × 3 array consisting of multi-port elements. The multi-port element is a four-port patch antenna that is shorted in the middle, the structure being novel itself as well. The validity of the method is verified by determining element-level port signals and impedances, and array-level element weights that maximize the pre-defined goals in a certain angular range. In this example, the goal is to achieve as wide gain coverage as possible. When the goal is achieved, the determined port signals and impedances are realized with matching and feeding networks, and reactive components to reduce the elements into single-feed antennas in practice. The realized array is manufactured and measured besides simulations. This array is compared to a reference array of the same size. The reference array consists of conventional patch antennas, and it is also manufactured and measured. The simulation and measurement results agree well with each other. The array designed with proposed model achieves a much wider coverage than the conventional array. The 3-dB coverage for this array is around ±68°.

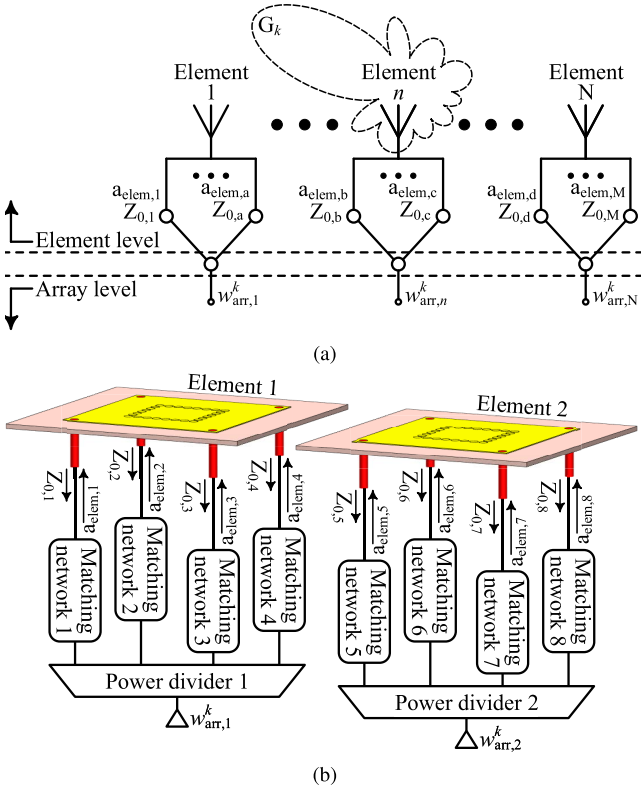

FIGURE 1. a) An array consisting of *N* elements and *M* feeding ports defined for a single objective G_k, and b) an example realization of a two-element array consisting of four-port elements.

II. THEORY OF THE MODEL AND METHOD

The proposed method is a major extension to the earlier works, where a multi-port antenna has been optimized in terms of port currents while maximizing the radiation efficiency [17], or the partial radiation efficiency in a certain angular range [18]. The earlier work [18] has covered optimization of single multi-port antennas and an array separately, whereas in this paper, we aim to optimize both antenna array and its multi-port antenna elements simultaneously. We create a model for determining the realized gain at different angles as a function of element-level port impedances and signals, and array-level weights. As an example, the proposed model is then used to find Pareto optimal solutions [19] by means of multi-objective genetic algorithm optimization.

A. MULTI-OBJECTIVE OPTIMIZATION MODEL

An antenna array consisting of multi-port elements is shown in Fig.1a. In total, there are N elements and M feeding ports in the array. Each port is characterized by element-level port signal $a_{\text{elem},m}$ and impedance $Z_{0,m}$. A single element may contain an arbitrary number of ports which is is illustrated in Fig. 1a. The element indexes a, b, c, and d ($1 < a < b < c < d < M$) may be chosen arbitrarily. Thus for example, element n has $c - b + 1$ ports according to the figure. Each element is fed with an array-level weight $w^k_{\text{arr},n}$ to allow the beam steering of the array to different angles. Here k denotes index at which angle θ_k and ϕ_k realized gain G_k is calculated.

Fig. 1b demonstrates how the multi-port element signals and impedances are achieved in practice.

Generally, the design of the system shown in Fig. 1 can be considered as a multi-objective optimization problem. In particular, using the realized gains at K different angles as objective functions enables mathematically formulating the problem as

$$\text{v-max } \vec{G}(\vec{x}) = \{G_1(\vec{x}_1) \cdots G_k(\vec{x}_k) \cdots G_K(\vec{x}_K)\}, \tag{1}$$

where v-max denotes identifying values for the decision variables $\vec{x}$ that correspond to a Pareto optimal solution to the vector-valued objective function $\vec{G}$. In this case,

$$\vec{x} = \{\vec{x}_1 \ldots \vec{x}_k \ldots \vec{x}_K\}, \tag{2}$$

where

$$\vec{x}_k = \{\boldsymbol{a}_{\text{elem}}, \mathbf{Z}_0, \boldsymbol{w}^k_{\text{arr}}\}. \tag{3}$$

In (3), vectors $\boldsymbol{a}_{\text{elem}}$, $\mathbf{Z}_0$, and $\boldsymbol{w}^k_{\text{arr}}$ contain the element-level port signals $a_{\text{elem},m}$ and impedances $Z_{0,m}$, and the array-level weights $w^k_{\text{arr},n}$, respectively. The variables $\boldsymbol{a}_{\text{elem}}$ and $\mathbf{Z}_0$ are shared among all the $\vec{x}_k$ denoting that a single element port is characterized by two decision variables. Each objective $G_k(\vec{x}_k)$ is fulfilled with a unique set of array weights meaning that each objective adds as many decision variables as there are elements. Thus, the total number of decision variables for M feeding ports, N elements, and K objectives is $2M + NK$.

Note that generally there does not exist feasible solution $\vec{x}$ that would maximize all the objective functions simultaneously. Hence, multi-objective optimization algorithms seek to identify Pareto optimal solutions: a feasible solution is Pareto optimal if no other feasible solution yields a better or equal value in all objective functions and strictly better at least in one objective function [19].

B. MODEL FOR REALIZED GAIN IN THE GENERAL CASE

The realized gain can be calculated as a function of the element-level port signals and impedances, and the array-level weights as follows. The definition of the realized gain at a single angle $\theta = \theta_k$ and $\phi = \phi_k$ is

$$G_k(\vec{x}_k) = \frac{\frac{1}{2\eta}|\vec{\boldsymbol{F}}(\vec{x}_k)|^2}{\frac{1}{4\pi}P_{\text{in}}(\vec{x}_k)}, \tag{4}$$

where η is the free-space impedance, $F_{\theta_k,\phi_k}(\vec{x}_k)$ is the electric far field at a single angle, and $P_{\text{in}}(\vec{x}_k)$ is the total input power of the array.

Generally, the total input power can be calculated as

$$P_{\text{in}} = \frac{1}{2}\boldsymbol{a}^{\text{H}}\boldsymbol{a}, \tag{5}$$

where $^{\text{H}}$ denotes the Hermitian transpose, and $\boldsymbol{a}$ is a column vector of length M containing the port signals a_m. Following [18], vector $\boldsymbol{a}$ is defined as

$$\boldsymbol{a} = \frac{1}{2}\mathbf{F}(\boldsymbol{U} + \mathbf{Z}_{\text{P}}\boldsymbol{I}) = \frac{1}{2}\mathbf{F}(\mathbf{Z}_{\text{A}} + \mathbf{Z}_{\text{P}})\boldsymbol{I} = \mathbf{B}\boldsymbol{I}, \tag{6}$$

where vector $\boldsymbol{I}$ contains the port currents i_m, $\mathbf{Z}_{\text{A}}$ is the multi-port antenna impedance matrix with a size of $M \times M$, and $\mathbf{F}$ and $\mathbf{Z}_{\text{P}}$ are diagonal matrices of the same size. The diagonal elements of these matrices are $F_{mm} = \left(\sqrt{\text{Re}\{Z_{0,m}\}}\right)^{-1}$ and $Z_{\text{P},mm} = Z_{0,m}$, respectively.

The squared absolute value of the far field can be computed in terms of port currents as

$$|\vec{\boldsymbol{F}}_{\theta_k,\phi_k}|^2 = \boldsymbol{I}\mathbf{R}^k_{\text{rad}}\boldsymbol{I}, \tag{7}$$

where $\mathbf{R}^k_{\text{rad}}$ is the radiation matrix and has a size of $M \times M$. The elements of the radiation matrix are defined as

$$(\mathbf{R}^k_{\text{rad}})_{ij} = \vec{\boldsymbol{K}}^*_i(\theta_k, \phi_k) \cdot \vec{\boldsymbol{K}}_j(\theta_k, \phi_k), \tag{8}$$

where $\vec{\boldsymbol{K}}_l(\theta_k, \phi_k)$ gives the relation between the far field at angle θ_k and ϕ_k and the current i_l at port l. For more information on vector $\vec{\boldsymbol{K}}_l(\theta_k, \phi_k)$, see [20]. Note that variants of the radiation matrix are also shown in [17], [18].

The previous equations lack information on how the current vector $\boldsymbol{I}$ depends on the element-level port signals $\boldsymbol{a}_{\text{elem}}$, and the element weights $\boldsymbol{w}^k_{\text{arr}}$ on the array level. We can rewrite $\boldsymbol{a}$ in (6) as

$$\boldsymbol{a} = \mathbf{A}_{\text{elem}}\boldsymbol{w}^k_{\text{arr}}, \tag{9}$$

where $\boldsymbol{w}^k_{\text{arr}}$ is a column vector of length N containing the array weights $w^k_{\text{arr},n}$, and $\mathbf{A}_{\text{elem}}$ is a matrix of size $M \times N$ with M non-zero elements. The remaining elements have zero values. The non-zero elements are defined such that $A_{\text{elem},mn} = a_{\text{elem},m}$, where port m belongs to element n. For example according to Fig. 1a, $A_{\text{elem},11} = a_{\text{elem},1}$, $A_{\text{elem},a1} = a_{\text{elem},a}$, and $A_{\text{elem},dN} = a_{\text{elem},d}$.

Setting (9) equal to (6) yields

$$\boldsymbol{I} = (\mathbf{B})^{-1}\mathbf{A}_{\text{elem}}\boldsymbol{w}^k_{\text{arr}} = \mathbf{C}_{\text{elem}}\boldsymbol{w}^k_{\text{arr}}, \tag{10}$$

which allows to express the gain as

$$G_k = \frac{4\pi}{\eta}\frac{\left(\boldsymbol{w}^k_{\text{arr}}\right)^{\text{H}}(\mathbf{C}_{\text{elem}})^{\text{H}}\mathbf{R}_{\text{rad}}\mathbf{C}_{\text{elem}}\boldsymbol{w}^k_{\text{arr}}}{\left(\boldsymbol{w}^k_{\text{arr}}\right)^{\text{H}}(\mathbf{A}_{\text{elem}})^{\text{H}}\mathbf{A}_{\text{elem}}\boldsymbol{w}^k_{\text{arr}}}. \tag{11}$$

This equation shows that the gain is dependent on the element-level port signals $a_{\text{elem,m}}$ and impedances $Z_{0,m}$, and the array weights $w^k_{\text{arr},n}$. Note that the realized gain has the form of a Rayleigh quotient, and the array weights maximizing the gain can be solved from a general eigenvalue problem provided that the element-level port signals and impedances are determined before the calculation. Thus, this formulation allows the number of optimization variables to be independent on the number of objectives.

C. MODEL FOR REALIZED GAIN WHEN A FIXED NUMBER OF PORTS ARE FED

The earlier definition of the realized gain assumes that all the ports are fed. In some cases, it may be beneficial that some of the ports are loaded reactively. This requires changes in the antenna impedance and the radiation matrix. The size of these matrices is reduced to correspond to the number of feeding ports. Fig. 2a shows the schematic presentation of

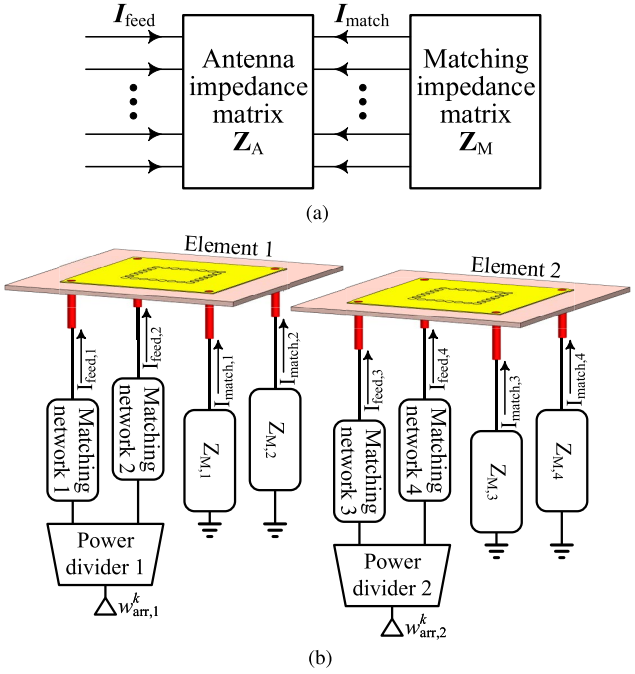

FIGURE 2. **(a) Circuit schematic of a multi-port antenna array where some port are active and others are passive. (b) A possible realization of a two-element array, with two active ports in each element.**

a situation where some ports of the multi-port antenna are fed. The remaining ports are loaded with matching elements. A possible realization is shown in Fig. 2b when two element ports are fed.

The multi-port antenna is characterized by its antenna impedance matrix $\mathbf{Z}_{\text{A}}$, whereas the matching elements are accounted for in the matching matrix $\mathbf{Z}_{\text{M}}$. The matching matrix is a diagonal matrix in which each diagonal element gives the impedance of the matching element at the corresponding port. The currents at the antenna ports can be divided into two categories: feeding ($\boldsymbol{I}_{\text{feed}}$) and matching ($\boldsymbol{I}_{\text{match}}$) currents. The goal is to find the relation between the feeding voltages ($\boldsymbol{U}_{\text{feed}}$) and currents ($\boldsymbol{I}_{\text{feed}}$) while making the relation independent of the matching currents. The relation is dependent on the matching elements though.

The aforementioned relation can be found by first partitioning the antenna impedance matrix into sub-matrices according to the feeding and matching ports:

$$\begin{bmatrix} \boldsymbol{U}_{\text{feed}} \\ \boldsymbol{U}_{\text{match}} \end{bmatrix} = \begin{bmatrix} \mathbf{Z}_{\text{A},11} & \mathbf{Z}_{\text{A},12} \\ \mathbf{Z}_{\text{A},21} & \mathbf{Z}_{\text{A},22} \end{bmatrix} \begin{bmatrix} \boldsymbol{I}_{\text{feed}} \\ \boldsymbol{I}_{\text{match}} \end{bmatrix}, \tag{12}$$

where for example $\mathbf{Z}_{\text{A},12} = \mathbf{Z}_{\text{A}}(\boldsymbol{m}_{\text{feed}}, \boldsymbol{m}_{\text{match}})$ gives the relation between $\boldsymbol{U}_{\text{feed}}$ and $\boldsymbol{I}_{\text{match}}$. Here $\boldsymbol{m}_{\text{feed}}$ and $\boldsymbol{m}_{\text{match}}$ are vectors containing the port indices of the feeding and matching ports, respectively. Note that a similar partition has been used in [21] although for a different purpose.

We can divide (12) into two equations:

$$\boldsymbol{U}_{\text{feed}} = \mathbf{Z}_{\text{A},11}\boldsymbol{I}_{\text{feed}} + \mathbf{Z}_{\text{A},12}\boldsymbol{I}_{\text{match}} \tag{13}$$

and

$$\boldsymbol{U}_{\text{match}} = \mathbf{Z}_{\text{A},21}\boldsymbol{I}_{\text{feed}} + \mathbf{Z}_{\text{A},22}\boldsymbol{I}_{\text{match}}. \tag{14}$$

The latter can be used in solving the relation between $\boldsymbol{I}_{\text{match}}$ and $\boldsymbol{I}_{\text{feed}}$, and applying the fact that

$$\boldsymbol{U}_{\text{match}} = -\mathbf{Z}_{\text{M}}\boldsymbol{I}_{\text{match}}, \tag{15}$$

where the minus sign comes as the result of the chosen current direction. When (15) is combined with (14) we obtain

$$\boldsymbol{I}_{\text{match}} = -(\mathbf{Z}_{\text{M}} + \mathbf{Z}_{\text{A},22})^{-1}\mathbf{Z}_{\text{A},21}\boldsymbol{I}_{\text{feed}} = \mathbf{D}\boldsymbol{I}_{\text{feed}}. \tag{16}$$

Applying (16) in (13) yields

$$\boldsymbol{U}_{\text{feed}} = (\mathbf{Z}_{\text{A},11} + \mathbf{Z}_{\text{A},12}\mathbf{D})\boldsymbol{I}_{\text{feed}} = \mathbf{Z}_{\text{A,r}}\boldsymbol{I}_{\text{feed}}. \tag{17}$$

This changes matrix $\mathbf{B}$ in (6), and it becomes

$$\mathbf{B}_{\text{r}} = \frac{1}{2}\mathbf{F}_{\text{r}}(\mathbf{Z}_{\text{A,r}} + \mathbf{Z}_{\text{P,r}}), \tag{18}$$

and now matrix $\mathbf{C}_{\text{elem}}$ in (10) is

$$\mathbf{C}_{\text{elem,r}} = (\mathbf{B}_{\text{r}})^{-1}\mathbf{A}_{\text{elem,r}}. \tag{19}$$

Radiation matrix can also be partitioned in a similar way

$$\mathbf{R}^k_{\text{rad}} = \begin{bmatrix} \mathbf{R}^k_{\text{rad},11} & \mathbf{R}^k_{\text{rad},12} \\ \mathbf{R}^k_{\text{rad},21} & \mathbf{R}^k_{\text{rad},22} \end{bmatrix}, \tag{20}$$

and we can write for the currents that

$$\begin{bmatrix} \boldsymbol{I}_{\text{feed}} \\ \boldsymbol{I}_{\text{match}} \end{bmatrix} = \begin{bmatrix} \mathbf{I}_{\text{id}} \\ \mathbf{D} \end{bmatrix} \left[\boldsymbol{I}_{\text{feed}}\right], \tag{21}$$

where $\mathbf{I}_{\text{id}}$ is an identity matrix having the same size as $\mathbf{D}$. Applying (20) and (21) in (7) yields

$$\left|\vec{\boldsymbol{F}}_{\theta_k,\phi_k}\right|^2 = \boldsymbol{I}^{\text{H}}_{\text{feed}}\mathbf{R}^k_{\text{rad,r}}\boldsymbol{I}_{\text{feed}}, \tag{22}$$

where $\mathbf{R}^k_{\text{rad,r}}$ is the reduced radiation matrix

$$\mathbf{R}^k_{\text{rad,r}} = \begin{bmatrix} \mathbf{I}_{\text{id}} \\ \mathbf{D} \end{bmatrix}^{\text{H}} \begin{bmatrix} \mathbf{R}^k_{\text{rad},11} & \mathbf{R}^k_{\text{rad},12} \\ \mathbf{R}^k_{\text{rad},21} & \mathbf{R}^k_{\text{rad},22} \end{bmatrix} \begin{bmatrix} \mathbf{I}_{\text{id}} \\ \mathbf{D} \end{bmatrix}. \tag{23}$$

The expression for gain in the case of aperture matched components is

$$G_k = \frac{4\pi}{\eta} \frac{\left(\boldsymbol{w}^k_{\text{arr,r}}\right)^{\text{H}} \left(\mathbf{C}_{\text{elem,r}}\right)^{\text{H}} \mathbf{R}^k_{\text{rad,r}} \mathbf{C}_{\text{elem,r}} \boldsymbol{w}^k_{\text{arr,r}}}{\left(\boldsymbol{w}^k_{\text{arr,r}}\right)^{\text{H}} \left(\mathbf{A}_{\text{elem,r}}\right)^{\text{H}} \mathbf{A}_{\text{elem,r}} \boldsymbol{w}^k_{\text{arr,r}}}. \tag{24}$$

When the single element has only one feed and the other ports are loaded with lumped elements for example, then the equation for realized gain in the earlier section becomes significantly simpler. As there is one feed per element, there is no need to separate element-level signals and array-level weights. It is sufficient to account for only the element-level port signals.

Since there is no need to consider the element-level weights, matrix $\mathbf{C}^k_{\text{elem,r}}$ can be replaced with matrix $(\mathbf{B}_{\text{r}})^{-1}$, and thus the realized gain in this special case is

$$G_k = \frac{4\pi}{\eta} \frac{(\boldsymbol{a}^k_{\text{feed}})^{\text{H}}((\mathbf{B}_{\text{r}})^{-1})^{\text{H}} \tilde{\mathbf{R}}^k_{\text{rad,r}} (\mathbf{B}_{\text{r}})^{-1} \boldsymbol{a}^k_{\text{feed}}}{(\boldsymbol{a}^k_{\text{feed}})^{\text{H}} \boldsymbol{a}^k_{\text{feed}}}. \tag{25}$$

D. EXTENSIONS TO THE MODEL

Above we have formulated our model with multiple objectives, each capturing the gain at a specific angle. However, the model can be extended to other types of problems as well. For example, the model can be used for a single-objective problem where the goal is maximizing the minimum of the realized gain at a certain angular range with or without sidelobe level constraints.

Although we do not consider the sidelobe levels for simplicity, there is no reason why the sidelobe levels could not be taken into account. Since the gain can be computed for a single angle it is straightforward to calculate those gain patterns that are required for the determination of the sidelobe levels.

The model is also applicable for determining the feeding network structures for sub-arrays provided that the sub-arrays have been simulated for scattering parameters and port-specific electric fields. Although we formulated the model for multi-port antenna elements, the model can be applied to arrays with single feed elements. Specifically with slight modifications, the model could also take into account the matching networks at the feeding ports as well. Furthermore, the model can be applied in antenna arrays where the elements are reconfigurable.

E. MODEL AS PART OF THE METHOD

Since the above models for gain can be defined to be dependent on element- and array-level variables, it is possible to optimize both the element and array at the same time. Thus, we utilize this model according to Fig. 3 showing the generalized design flow of the method.

The first step in the method is to decide the minimum requirement for the gain at different steering angles of the array. Then, a set of objective gains at different angles are chosen depending on the gain requirements. The next step in the method is choosing a multi-port antenna element and an array configuration. The array is simulated to obtain port-specific electric fields and antenna impedance parameters.

These fields and parameters are then exported into an optimizer to to define the objective gains in terms of the element-level port signals and impedances, and the array level weights (decision variables) with the proposed model. Next, the optimizer performs a multi-objective optimization for the chosen objective set. Since the number of decision variables and objectives might be large, and the problem is non-linear (i.e., the gains are non-linear functions of element port signals and impedances, and array weights), a genetic algorithm (GA) producing the Pareto optimal solutions for the objectives is a viable choice.

Generally, Pareto optimality means that no objective can be improved without degrading another [19]. Thus in this work, Pareto optimality means that gain at one angle cannot be increased without decreasing the gain at another angle. Producing Pareto optimal solutions can be valuable in antenna array design since the designer obtains information

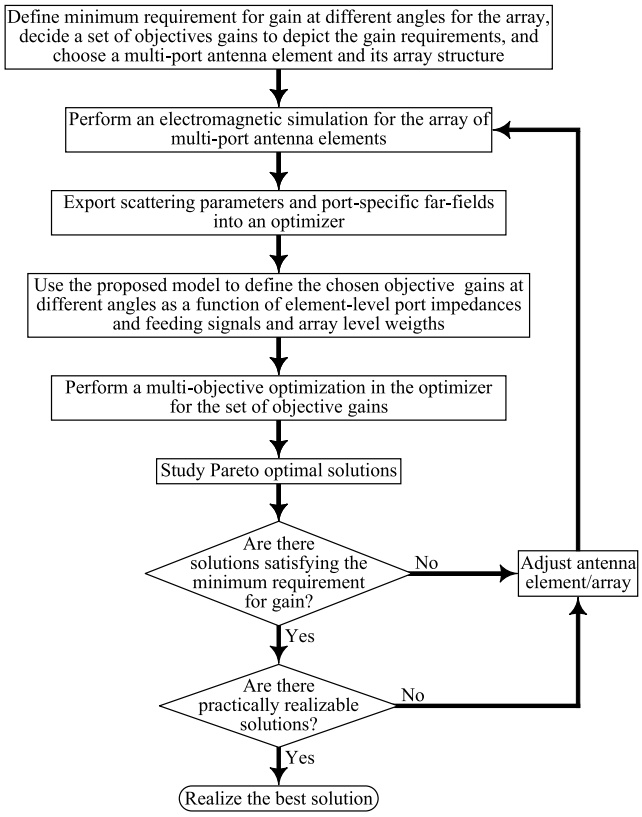

FIGURE 3. A diagram of the design flow of the proposed method.

on the trade-offs between different objectives. For example, the designer can choose how much broadside gain is traded for wider beam scanning range. Furthermore, the solutions in the Pareto front can be used as initial points for further optimization. If some Pareto optimal solutions satisfy the minimum gain requirements and are practically realizable, the best solution among those solutions is chosen to be manufactured. When there are no feasible solutions, then the antenna element or the array is adjusted, and another EM-simulation is required.

F. ADVANTAGES OVER CONVENTIONAL DESIGN METHODS

The conventional methods aim to design an antenna element with proper radiation properties such as a wide angle pattern, and then utilize it in an antenna array with progressive phase shifts. Thus, the design of a single element and the array weights are separate processes. Our model allows simultaneous tailoring of both the element and array patterns which gives a remarkable benefit compared to the conventional methods.

Apart from reconfigurable antenna elements, the conventional methods rely heavily on EM-simulations in achieving optimal element patterns, whereas the method developed here can also tailor the single element pattern through the optimization of the element-level signals and port impedances. Thus, the proposed method requires less

structural optimization. Ideally, a single EM-simulation is required with the proposed method.

Furthermore, our proposed model enables the design of unique antenna elements only by changing the feeding structure while in the conventional design, this would require physical changes in the antenna structure. Thus in our case, the corner elements can more easily be designed to obtain the best possible operation for the array.

III. APPLICATION OF THE MODEL IN AN EXAMPLE CASE

In this part, we show how an antenna array consisting of multi-port antenna elements can be optimized with the proposed method. We choose a single antenna array consisting of 3×3 multi-port elements. Although the elements are identical in the design example, the optimization allows the elements to be different. The chosen antenna array is optimized with different gain objective sets to demonstrate the method.

A. CHOSEN ANTENNA STRUCTURE

The chosen multi-port antenna element and the array are shown in Fig. 4. The element is designed to operate at 2.5 GHz. The substrate structure and the via types used for the elements are shown in Fig. 4a, and it consists of two Rogers RO4350B slabs and two Rogers 4450F slabs having thicknesses of 0.762 mm and 0.101 mm, respectively. In total, there are three layers (antenna, ground, feeding) of copper.

All the elements in the array are identical and, Fig. 4b shows the antenna layer of element one. It consists of a 40 mm by 40 mm square metal patch backed by a uniform metal sheet (ground layer) separated by distance of 0.964 mm. The metal patch is connected to the ground layer with several shorting vias ($d = 0.95$ mm) arranged in a square shape in the middle. The side length of the grounding is varied to control the resonance frequency of the element, and is set to 16.6 mm. The metal patch is connected to the signal layer with feeding vias ($d = 0.50$ mm) from each corner. The signal layer is shown in Fig. 4c, and the feeding vias connect to 50 -Ω microstrip lines. At this stage of the design process, the microstrip lines are fed with waveguide ports in the electromagnetic simulator. Effectively, the element can be seen consisting of four planar-inverted F-antennas (PIFA) sharing a direct galvanic connection.

The whole array shown in Fig. 4d is arranged into 3×3 configuration with element spacing being 0.375λ (45 mm) at 2.5 GHz. This element spacing was chosen to maintain relatively low sidelobe levels without setting them as objectives. Figure also shows how different elements, and their ports are numbered. The starting port number of element n is $4(n-1)+1$.

B. PARETO OPTIMAL SOLUTIONS FOR DIFFERENT OBJECTIVE SETS

We first perform an electromagnetic simulation for the array structure described in the earlier section to obtain Pareto optimal solutions for a few different objective sets. The whole array structure consisting of $4 \cdot 9 = 36$ ports is simulated

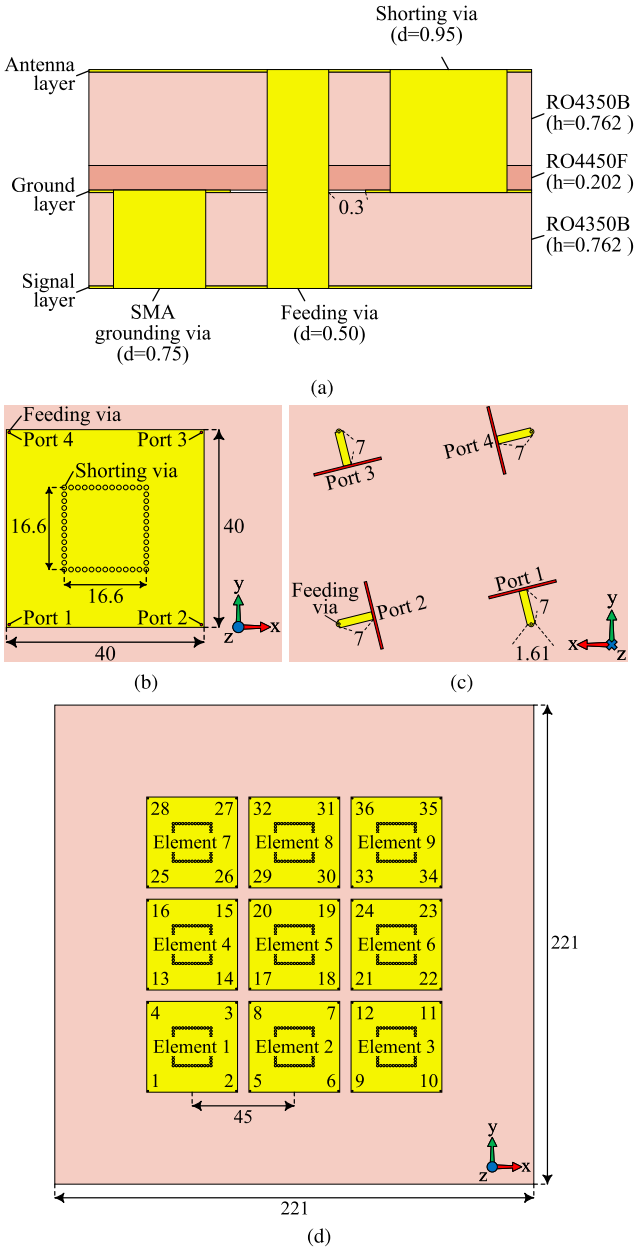

FIGURE 4. The physical structure of the design example. (a) The general cross-section of substrate structure showing the different vias used in the example. (b) Antenna and (c) feeding layer of element one. (d) The array configuration shows the overall dimensions, and element and port numbers. The dimensions are in millimeters.

in CST Studio Suite. The CST gives port-specific electric far fields and impedance parameters which are then exported for the optimizer to be used in the calculation of objective gains. The optimizer is constructed in MATLAB by applying readily implemented multi-objective genetic algorithm function (*multiobjga*) available through the Global Optimization Toolbox. The objective functions (gains) required by the *multiobjga* are implemented in MATLAB with the gain model discussed in the earlier section. When the objective functions have been constructed, the Pareto solutions of the objectives may be produced in MATLAB.

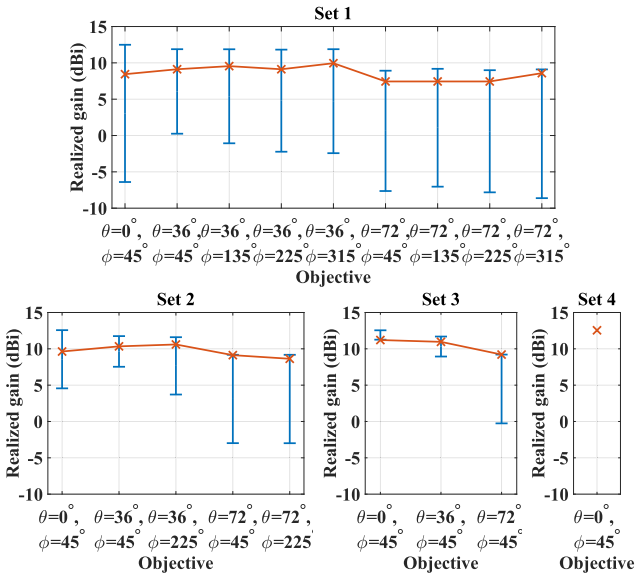

FIGURE 5. The maximum and minimum realized gain (blue bar) for different objectives and objective sets among Pareto points, and an example solution (orange cross).

In order to reduce the number of variables, we constrain ourselves to a situation where each element is identical in terms of port impedances and element-level signals. Thus, the number of element-level variables reduce to $2 \cdot 4 = 8$ instead of $2 \cdot 4 \cdot 9 = 72$. We also use (11) for calculating the objective gain which allows the calculation of array weights with the help of Rayleigh quotient when no constraints are set. Thus, the number of variables optimized with the genetic algorithm can be made independent of the number of objectives, and this results in just eight element-level variables.

The Pareto solutions are studied for the aforementioned array and for four different objective sets. The objective sets include different number of objectives. Fig. 5 shows these objective sets and the maximum and minimum realized gain for each objective among the Pareto solutions. The figure also shows an optimized example of a single Pareto solution. This example is the result of a trade-off optimization based on the maximum values of the objectives residing on the Pareto front.

Objective sets 1–3 include three different θ angles (0°, 36° and 72°). The difference between the sets is the range of ϕ angles. Set 1 has a full ϕ range with resolution being 90 degrees, while set 2 is limited the same way as a linear array. Set 3 is even more limited, and set 4 is limited to a single objective, which is the realized gain in the broadside direction.

Fig. 5 clearly indicates that the more the objective set is constrained the better the realized gain. For example in set 1, the realized gain varies between 7.4 dBi and 10.0 dBi, and in set 3 the gain is 9.2 dBi at minimum and denotes an increase of 1.8 dBi. Sets 1–3 also show that a wide angle scanning can be achieved in all the cases since the differences in the realized gains are within 3 dB. Thus, all the sets achieve at least scanning range from 0° to 72° which is a major improvement when compared to a conventional patch antenna array that can approximately achieve a 3-dB scanning range of $\theta = 0° - 50°$ at most.

TABLE 1. Element level port feeding signals and impedances for optimized 3 × 3 array with different objective sets.

Set	Port	$\lvert a_{\text{elem}} \rvert$ (dB)	Z_{P} (Ω)
1	1	−45	j19.7
	2	−445	−j43.9
	3	−434	j15.9
	4	0	16.1 + j76.8
2	1	0	33.0 + j134.1
	2	−51	−j90.3
	3	−48	j114.5
	4	−49	−j54.5
3	1	0	38.9 + j152.3
	2	−494	−j92.1
	3	−441	j132.6
	4	−56	−j103.5
4	1	−526	0
	2	−0	29.5 + j158.4
	3	−476	−j106.0
	4	0	29.5 + j158.3

Although the results are very different for sets 1–3, the port feeding scheme shown in Table 1 is similar. In all the cases, the optimization has found a solution favoring a single port excitation. For example in case 2, the feeding signal amplitude is signifigantly larger in port 1 than in ports 2–4 denoting that those ports are effectively passive. In sets 1–3, the feeding port impedance can easily be matched, and the passive ports can be replaced with inductors or capacitors. A larger difference is seen, when set 4 is compared to the other sets. In set 4, two ports with a realizable port impedance are fed with an equal amplitude, and the two other ports can be replaced with a short or a capacitor.

The results for these objectives should be viewed critically since the angle resolution is low. Thus, the objective sets might find solutions that give a low performance defined at angles outside the objectives. This issue is carefully addressed in the following section.

C. REALIZATION

The previous section showed that the chosen element can be optimized for different objectives by only changing the feeding signal values and the port impedances without affecting the physical structure. However, the chosen objective sets are coarse in terms of angle samples. Thus, the number of objectives is increased. We choose to realize the most difficult case in our opinion which is the objective set 1. To avoid low performance in angles not captured by the objectives, we optimize the realized gain with 9° steps for both θ and ϕ angles.

TABLE 2. Port impedances of a single element for the optimized 3 × 3 array with different objective sets.

Port	Set 1: Z_P (Ω)
1	16.9 + j77.8
2	0.0 + j19.8
3	0.0 − j45.0
4	0.0 + j16.5

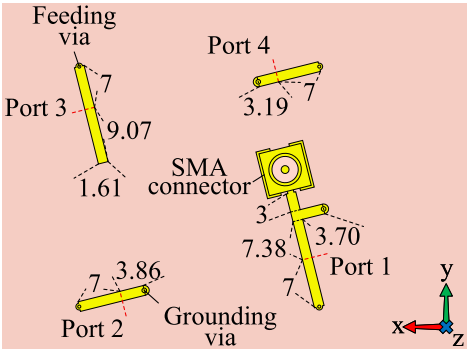

FIGURE 6. Matching network for realizing the required port impedances.

Since the results in the earlier section indicate that a single-feed element is preferable, we use these elements. This allows even faster optimization process since (25) is used for the calculation of the realized gain. Thus, the variables to optimize include the feeding port impedance and the non-fed port reactances. Furthermore, every element is considered identical as well. Note that the optimization with multiple feeding ports is possible but the optimization is a trade-off between the angle resolution and the time taken to optimize.

After the optimization, the realized gain varies between 7.4 dBi and 10.6 dBi in the angular range. The minimum gain remains the same as for the coarser angular range. However, the upper limit is 0.6 dB higher. The port impedances of single elements are shown in Table 2. The table shows that the reactive element values for ports 2–4 are j19.8 Ω, −j45.0 Ω, and j16.5 Ω, respectively. The feeding port impedance should be (16.9 + j77.8) Ω. In ports 2–4, the reactive elements are realized with open ended or shorted microstrip line sections. A matching network is used to transform the required feeding port impedance to the 50-Ω input impedance being the impedance of the surface-mount SMA connector. The physical structure, the matching network, and the reactive elements are shown in Fig. 6 with their dimensions.

IV. RESULTS

We use a conventional patch antenna array as the reference, and its dimensions are shown in Fig. 7. The substrate structure is the same as for the proposed array. The patch antenna is designed to operate at 2.5 GHz and the array spacing is 45 mm as well.

A. SIMULATED RESULTS

Both the proposed and reference arrays were simulated and designed with CST Studio Suite. The results that are shown

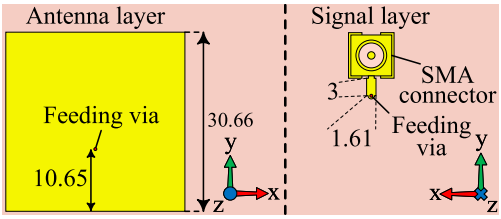

FIGURE 7. Antenna and signal layer of the reference antenna element.

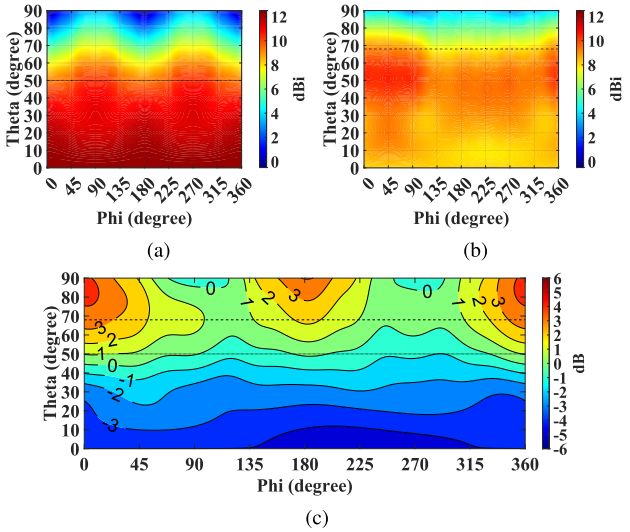

FIGURE 8. The simulated maximized realized gain of (a) the reference and (b) the proposed arrays, and (c) the difference in the realized gains at different angles at 2.5 GHz. The dotted and dashed lines show the 3dB scanning range of the reference and the proposed arrays, respectively.

have been processed in MATLAB. Fig. 8 shows the maximized realized gain at different angles for both the design example and the reference. We can see that the trade-off in increasing the scanning range is the reduction of the realized gain at small scanning angles. However, the benefits outweigh this reduction since the realized gain of the design example is even 3 dB better at large scanning angles than for the reference. The proposed array achieves a 3-dB scanning range of 68° which is 18° larger than that of the proposed array.

One reason for the flatter gain response for the proposed array can be seen in Fig. 9 showing the radiation efficiencies of both the arrays at different angles when the realized gain is maximized. The proposed design has a flatter radiation efficiency over the scanning range, and at angles where the reference array has dips, the radiation efficiency is improved by over 0.5 dB.

The other reason for the flatter gain is that the matching of the proposed array favors larger steering angles. The total active reflection coefficient (TARC) at different steering angles is shown in Fig. 10. TARC is a measure of the overall matching when all the feeding ports are taken into account. For an N-element array it is defined as [22]

$$\mathrm{TARC} = \sqrt{\frac{\mathbf{a}^{\mathrm{H}}\mathbf{S}^{\mathrm{H}}\mathbf{S}\boldsymbol{a}}{\boldsymbol{a}^{\mathrm{H}}\boldsymbol{a}}}, \tag{26}$$

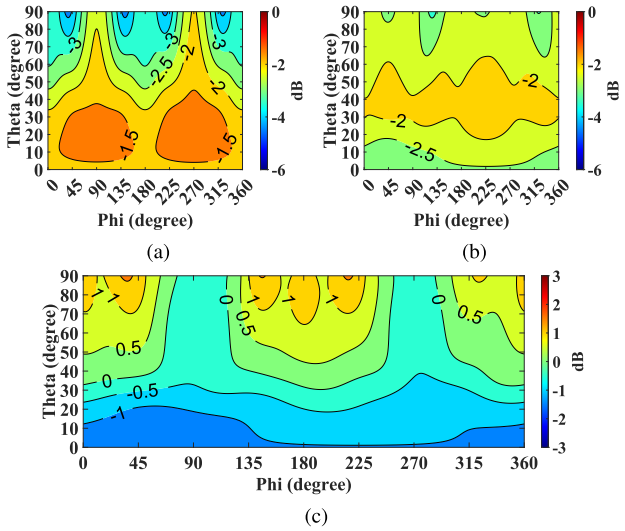

FIGURE 9. The simulated radiation efficiency of (a) the reference and (b) the proposed arrays, and (c) the difference in the efficiencies at different angles at 2.5 GHz.

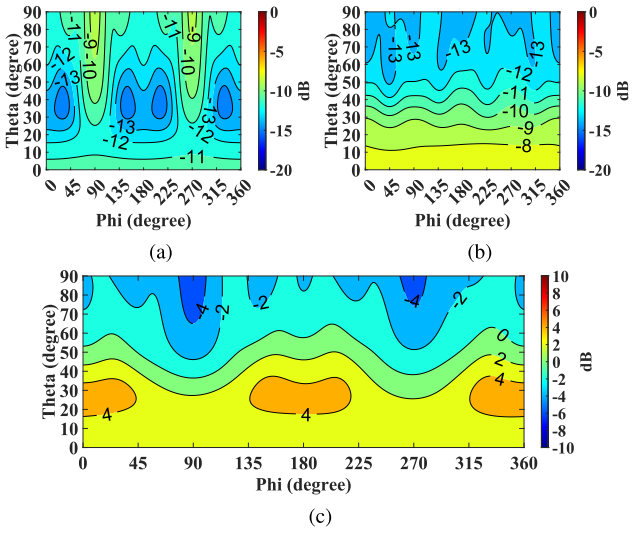

FIGURE 10. The simulated total active reflection coefficient of (a) the reference and (b) the proposed arrays, and (c) the difference of the reflection coefficients at different angles at 2.5 GHz.

where $\mathbf{S}$ is the array scattering matrix of size $N \times N$, and $\boldsymbol{a}$ is column vector containing the array weights. At over 50 degree angles, TARC is below -11 dB which is less than at the broadside where the TARC is above -8 dB. When compared to the reference case, we can see that the TARC of the proposed array outperforms the reference at larger steering angles.

B. MEASUREMENTS

The fabricated reference and proposed antenna arrays are shown in Fig. 11. The measurements of the far fields were carried out in Aalto University facilities using MVG StarLab 6-GHz equipment. The fields have been measured at 2.519 GHz due to the frequency shift of both designs. Fig. 12 shows the simulated and measured S-parameters of both

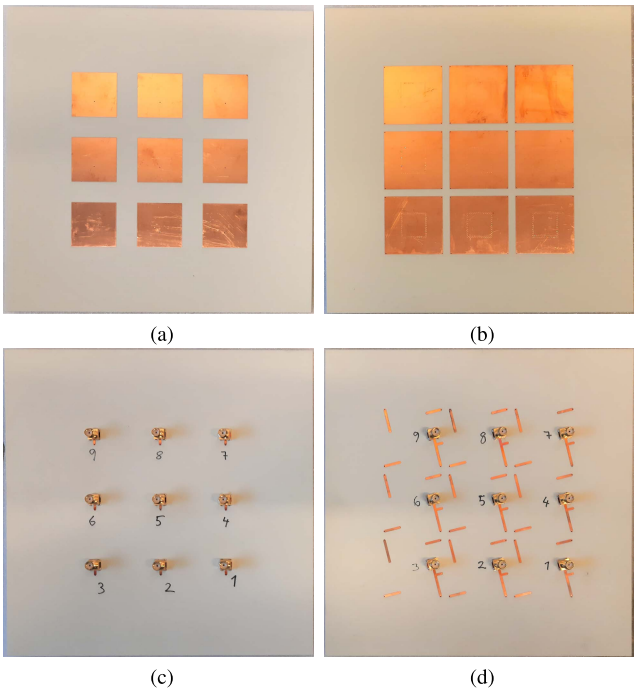

FIGURE 11. Manufactured (a),(c) reference and (b),(d) proposed antenna array.

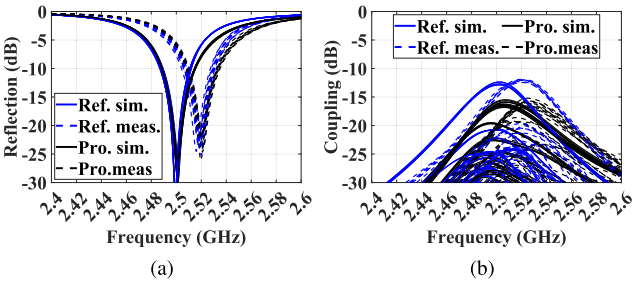

FIGURE 12. The simulated and measured S-parameters of the manufactured antenna arrays.

arrays, and the shift is clearly visible from the figure. The error in the resonant frequency is less than 1 %. Since the same frequency shift is observable in both designs, the most probable reason for this shift is that the fabricated arrays have a lower permittivity than what was used in the simulations. The error in the permittivity is within the tolerance given by the manufacturer.

The measurement results for the optimized realized gains are shown in Fig. 13c. The measurement results were obtained by combining the measured individual field patterns in MATLAB by weighting each field with the same array weights as in the simulations. The measured results agree well with their simulated counterparts. The 3-dB scanning ranges are exactly the same as in the simulations.

The measured TARCs are shown in Fig 14. The array scattering parameters were measured at 2.519 GHz, and the TARCs have also been calculated with the same array weights as in the simulations. The measured TARCs also agree well with their simulated counterparts.

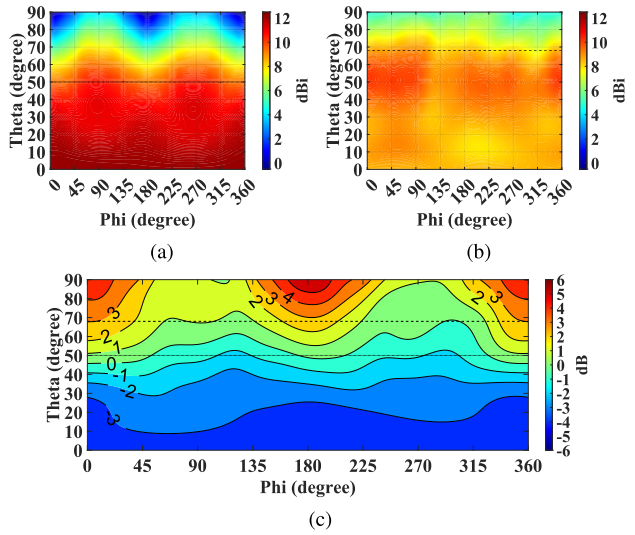

FIGURE 13. The measured maximized realized gain of (a) the reference and (b) the proposed arrays, and (c) the difference in the realized gains at different angles at 2.519 GHz. The dotted and dashed lines show the 3dB scanning range of the reference and the proposed arrays, respectively.

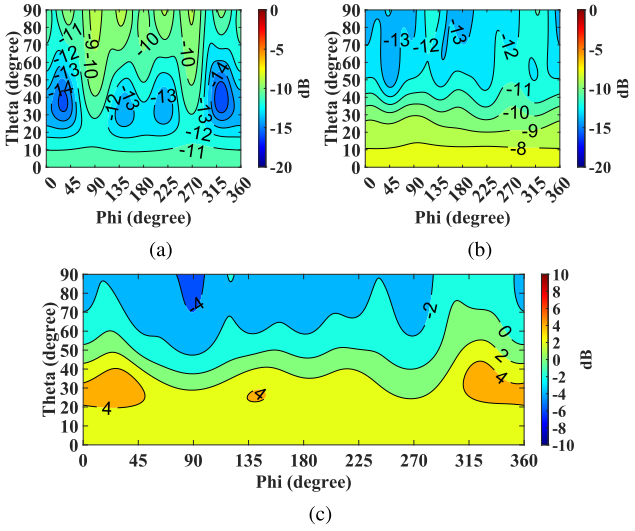

FIGURE 14. The measured total active reflection coefficient of (a) the reference and (b) the proposed arrays, and (c) the difference of the reflection coefficients at different angles at 2.519 GHz.

V. CONCLUSION

In this paper, we developed a method to simultaneously optimize an array consisting of multi-port antenna elements in terms of the realized gain in a given angular range. The method utilizes a non-linear multi-objective model that enables defining realized gain at certain angular points in terms of element-level port signals and impedances, and array-level weights. The method finds Pareto optimal solutions which are studied to choose the best realizable option for the given angular range. The validity of the method was verified with a practical design example that was compared to a reference patch antenna array of the same size. Both the simulation and measurement results show that the design example outperforms the reference array since the scanning range is increased from 50° to 68°.

The design example showed that the method is a promising alternative to conventional design methods. The method ideally requires a single EM-simulation instead of multiple iterations since the element-level variables allow flexible design of the elements without changing the physical structure. Furthermore, the proposed method is major extension to the existing methods for arrays composed of multi-port antenna elements/subarrays since the proposed method can separate element- and array-level excitations thus truly allowing simultaneous design of an array and its elements.

REFERENCES

[1] A. K. Vallappil, M. K. A. Rahim, B. A. Khawaja, N. A. Murad, and M. G. Mustapha, "Butler matrix based beamforming networks for phased array antenna systems: A comprehensive review and future directions for 5G applications," *IEEE Access*, vol. 9, pp. 3970–3987, 2021.

[2] Y.-B. Kim, S. Lim, and H. L. Lee, "Electrically conformal antenna array with planar multipole structure for 2-D wide angle beam steering," *IEEE Access*, vol. 8, pp. 157261–157269, 2020.

[3] G. Yang, Y. Zhang, and S. Zhang, "Wide-band and wide-angle scanning phased array antenna for mobile communication system," *IEEE Open J. Antennas Propag.*, vol. 2, pp. 203–212, 2021.

[4] B.-F. Sun, X. Ding, Y.-F. Cheng, and W. Shao, "2-D wide-angle scanning phased array with hybrid patch mode technique," *IEEE Antennas Wireless Propag. Lett.*, vol. 19, no. 4, pp. 700–704, Apr. 2020.

[5] G. Gao, X. Ding, Y. Cheng, and W. Shao, "Dual-polarized wide-angle scanning phased array based on mutimode patch elements," *IEEE Antennas Wireless Propag. Lett.*, vol. 18, no. 3, pp. 546–550, Mar. 2019.

[6] Z. Jiang, S. Xiao, Z. Yao, and B.-Z. Wang, "A planar ultrawideband wide-angle scanning array loaded with polarization-sensitive frequency-selective surface structure," *IEEE Trans. Antennas Propag.*, vol. 68, no. 11, pp. 7348–7357, Nov. 2020.

[7] B. Wang, X. Q. Lin, L. Y. Nie, and D. Q. Yu, "A broadband wide-scanning planar phased array antenna with equivalent circuit analysis," *IEEE Antennas Wireless Propag. Lett.*, vol. 19, no. 12, pp. 2154–2158, Dec. 2020.

[8] W. Dong, Z.-H. Xu, X.-H. Liu, L.-S.-B. Wang, and S.-P. Xiao, "Modular subarrayed phased-array design by means of iterative convex relaxation optimization," *IEEE Antennas Wireless Propag. Lett.*, vol. 18, no. 3, pp. 447–451, Mar. 2019.

[9] P. Rocca, L. Poli, A. Polo, and A. Massa, "Optimal excitation matching strategy for sub-arrayed phased linear arrays generating arbitrary-shaped beams," *IEEE Trans. Antennas Propag.*, vol. 68, no. 6, pp. 4638–4647, Jun. 2020.

[10] J. I. Echeveste, M. A. G. de Aza, and J. Zapata, "Shaped beam synthesis of real antenna arrays via finite-element method, Floquet modal analysis, and convex programming," *IEEE Trans. Antennas Propag.*, vol. 64, no. 4, pp. 1279–1286, Apr. 2016.

[11] S. Lei, Y. Yang, H. Hu, Z. Zhao, B. Chen, and X. Qiu, "Power gain optimization method for wide-beam array antenna via convex optimization," *IEEE Trans. Antennas Propag.*, vol. 67, no. 3, pp. 1620–1629, Mar. 2019.

[12] Y. Liu, M. Li, R. L. Haupt, and Y. J. Guo, "Synthesizing shaped power patterns for linear and planar antenna arrays including mutual coupling by refined joint rotation/phase optimization," *IEEE Trans. Antennas Propag.*, vol. 68, no. 6, pp. 4648–4657, Jun. 2020.

[13] Q. Wang, J. Yang, Y. Tang, R. Gao, and S. Liu, "Optimization method for pattern synthesis of sparse planar arrays considering mutual coupling and nonoverlapping constraint," *IEEE Trans. Antennas Propag.*, vol. 68, no. 8, pp. 6032–6038, Aug. 2020.

[14] P. Gu, Z. He, J. Xu, K. W. Leung, and R. S. Chen, "Design of wide scanning sparse planar array using both matrix-pencil and space-mapping methods," *IEEE Antennas Wireless Propag. Lett.*, vol. 20, no. 2, pp. 140–144, Feb. 2021.

[15] Y. Gong, S. Xiao, and B.-Z. Wang, "An ANN-based synthesis method for nonuniform linear arrays including mutual coupling effects," *IEEE Access*, vol. 8, pp. 144015–144026, 2020.

[16] R. T. Maximidis, D. Caratelli, G. Toso, and A. B. Smolders, "Design of overlapped subarrays based on aperture reactive loading," *IEEE Trans. Antennas Propag.*, vol. 68, no. 7, pp. 5322–5333, Jul. 2020.

[17] R. Kormilainen, J.-M. Hannula, T. O. Saarinen, A. Lehtovuori, and V. Viikari, "Realizing optimal current distributions for radiation efficiency in practical antennas," *IEEE Antennas Wireless Propag. Lett.*, vol. 19, no. 5, pp. 731–735, May 2020.
[18] R. Kormilainen, A. Lehtovuori, and V. Viikari, "A method for tailoring the gain pattern of a single antenna element," *IEEE Open J. Antennas Propag.*, vol. 2, pp. 431–438, 2021.
[19] S. Koziel and A. Pietrenko-Dabrowska, "Fast multi-objective optimization of antenna structures by means of data-driven surrogates and dimensionality reduction," *IEEE Access*, vol. 8, pp. 183300–183311, 2020.
[20] S. Otto, S. Held, A. Rennings, and K. Solbach, "Array and multiport antenna farfield simulation using EMPIRE, MATLAB and ADS," in *Proc. Eur. Microw. Conf. (EuMC)*, Sep. 2009, pp. 1547–1550.
[21] J. Weber, C. Volmer, K. Blau, R. Stephan, and M. A. Hein, "Miniaturisation of antenna arrays for mobile communications," in *Proc. Eur. Microw. Conf.*, Oct. 2005, p. 4.
[22] M. Manteghi and Y. Rahmat-Samii, "Broadband characterization of the total active reflection coefficient of multiport antennas," in *IEEE Antennas Propag. Soc. Int. Symp. Dig. Held Conjunct With, USNC/CNC/URSI North Amer. Radio Sci. Meeting*, Jun. 2003, pp. 20–23.

RIKU KORMILAINEN received the B.Sc. (Tech.) and M.Sc. (Tech.) degrees in electrical engineering from Aalto University, Espoo, Finland, in 2016 and 2018, respectively, where he is currently pursuing the D.Sc. (Tech.) degree with the Department of Electronics and Nanoengineering, School of Electrical Engineering.

He has been working with the Department of Electronics and Nanoengineering, School of Electrical Engineering, Aalto University, since 2018. His current research interests include multi-port antennas, patch antennas, and antenna arrays.

ANU LEHTOVUORI received the M.Sc. (Tech.) and Lic.Sc. (Tech.) degrees in electrical engineering from the Helsinki University of Technology, Espoo, Finland, in 2000 and 2003, respectively, and the D.Sc. (Tech.) degree in electrical engineering from Aalto University, Espoo, in 2015. She is currently a University Lecturer in circuit theory with the School of Electrical Engineering, Aalto University. Her current research interests include electrically small antennas, multiport antennas, and design of antennas for mobile devices.

JUUSO LIESIÖ is currently an Associate Professor of management science at the Aalto University School of Business and a Visiting Fellow of the Loughborough University School of Business and Economics. His research has been published in some of the leading journals in the field, such as *European Journal of Operational Research*, *Operations Research*, *Omega - The International Journal of Management Science*, *Technological Forecasting & Social Change*, and *Decision Analysis*. His research interests include decision analysis and prescriptive analytics with a focus on optimization approaches for handling incomplete preference information and uncertainties in decision support as well as on axiomatic preference theory. This research has been widely applied in practice, for instance, to support resource allocation decisions in environmental management, infrastructure asset management, and production planning.

VILLE VIIKARI (Senior Member, IEEE) received the Master of Science (Tech.) and Doctor of Science (Tech.) degrees (Hons.) in electrical engineering from the Helsinki University of Technology (TKK), Espoo, Finland, in 2004 and 2007, respectively.

He is currently a Professor and the Deputy Head of Department with the Aalto University School of Electrical Engineering, Espoo. From 2001 to 2007, he was with the Radio Laboratory, TKK (now part of Aalto University), where he studied antenna measurement techniques at submillimeter wavelengths and antenna pattern correction techniques. From 2007 to 2012, he was a Research Scientist and a Senior Scientist with the VTT Technical Research Centre, Espoo, where his research included wireless sensors, RFID, radar applications, MEMS, and microwave sensors. He was appointed as an Assistant Professor at Aalto University, in 2012. He has authored or coauthored about 85 journal articles and 90 conference papers. He is an inventor in 14 granted patents. His current research interests include antennas for mobile devices and networks, antenna clusters and coupled arrays, RF-powered devices, and antenna measurement techniques.

Dr. Viikari is a Regional Delegate of EurAAP. He was a recipient of the Young Researcher Award of the Year 2014, presented by the Finnish Foundation for Technology Promotion and the IEEE Sensors Council 2010 Early Career Gold Award.